

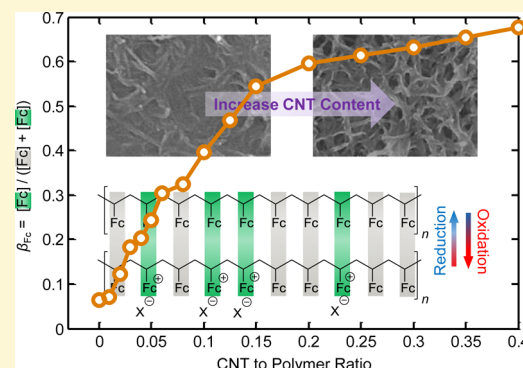
Enhanced Redox Transformation Efficiency in Unconjugated Electroactive Polymer/Carbon Nanotube Hybrids

Xianwen Mao, Esther H. Yan, Gregory C. Rutledge, and T. Alan Hatton*

Department of Chemical Engineering, Massachusetts Institute of Technology, 77 Massachusetts Avenue, Cambridge, Massachusetts 02139, United States

S Supporting Information

ABSTRACT: The mechanism for the redox activity of electroactive polymers (EAPs) with unconjugated backbones (e.g., polyvinylferrocene, PVFc) is fundamentally different from that of intrinsically conducting polymers. Here we investigate, for the first time, the redox transformation efficiency (RTE) of unconjugated EAPs with discrete electron donor/acceptors. We find that the RTE of PVFc can be modulated systematically by incorporation of carbon nanotubes (CNTs) via a facile and controllable solution process. Furthermore, we show that the improvement in the RTE of PVFc translated to enhanced performance of PVFc-based applications, such as energy storage, electrochemically responsive heterogeneous catalysis, and enzymatic biosensing. Our study provides valuable insights into the charge transport mechanism of unconjugated EAP/nanocarbon hybrids and the accelerated electron transfer kinetics by incorporation of materials with a high density of electronic states near the Fermi level. Moreover, this report suggests a generalizable strategy to modulate the accessibility and utilization of discrete redox moieties in unconjugated EAPs through creation of a heterogeneous nanostructure with a polymer-coated porous conducting framework that will simultaneously facilitate electron and ion transport processes.



INTRODUCTION

Electroactive polymers (EAPs) are attracting widespread interest in many research areas, such as organic electronics,¹ molecular sensing,² energy storage,³ drug delivery,⁴ and neural interface technologies.⁵ Better control over the redox transformation efficiency (RTE) and elucidation of the charge transport mechanism are the main barriers to such applications.^{1–9} EAPs are categorized into two classes: intrinsically conducting polymers (ICPs) and redox polymers (RPs).^{10,11} ICPs, such as polyaniline (PANI), possess conjugated backbones that undergo redox reactions and exhibit electron conducting behavior similar to that of metals.¹⁰ In contrast, RPs such as polyvinylferrocene (PVFc) have unconjugated backbones that do not participate in the redox transformation; only the pendent, discrete redox moieties can accept or donate electrons. RPs are localized-state conductors,^{10–12} and electron transport occurs through a diffusive process that relies on sequential electron hopping between adjacent redox groups and restricted physical motions of molecular chains.^{6–9,13}

Due to these distinct characteristic differences between ICPs and RPs, their RTEs should be defined differently. For ICPs, the parameter adopted for describing the RTE is the fraction (α) of electronic charge each monomer shares upon oxidation or the reciprocal of the number of monomer units required to donate or accept one electron.^{14–16} As an example, Figure 1a shows the redox mechanism of PANI and its α number. It

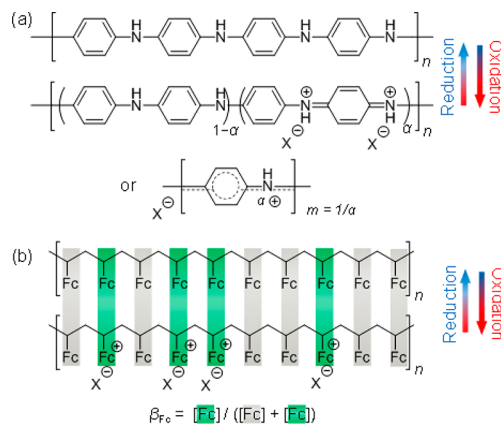


Figure 1. Redox transformation mechanisms of (a) PANI and (b) PVFc (green and gray boxes indicate active and inert Fc moieties, respectively). X^- denotes a generic counterion.

should be noted that there is not a unique α value for each type of ICP because α , and thus the RTE, depends strongly on the nature and concentration of dopants associated with the ICP. Determination of α for ICPs is not trivial and sometimes requires the use of an internal reference.^{14–16} For instance, with

Received: October 13, 2015

Revised: December 22, 2015

Published: January 5, 2016

certain types of dopants, α values of 0.25, 0.5, and 0.46 have been reported for thiophene-,¹⁴ aniline-,¹⁵ and pyrrole¹⁶-based ICPs, respectively, on conversion between certain redox states. For RPs, identification of α is straightforward since each monomeric unit contains chemically identifiable redox sites that can only donate or accept an integer number of electrons. For instance, when oxidized, one monomeric unit in PVFc carries one electron and thus for this polymer $\alpha = 1.0$.

In the case of RPs, another important but overlooked property that governs the RTE is the fraction of “active” redox centers. Using PVFc as an example, its RTE should be described by the ratio of the active to the total number of ferrocene (Fc) moieties (Figure 1b); this ratio is denoted as β_{Fc} hereafter. Not all redox sites are accessible for redox transformation in RPs. First, RPs have significantly lower electrical conductivities than do ICPs (e.g., $\sim 10^{-5}$ – 10^{-7} S/cm for PVFc¹⁷ versus $\sim 10^0$ – 10^2 S/cm for PANI).¹⁸ Second, RP structures are frequently nonporous, with limited polymer/electrolyte interfacial contact, which hinders ion intercalation into the polymer film; such intercalation is necessary to effect the redox reactions.^{9,19,20}

Here we find that incorporation of carbon nanotubes (CNTs) within PVFc films permits systematic modulation of the RTE of PVFc (i.e., β_{Fc}) as a function of the CNT-to-polymer mass ratio ($r_{\text{C/P}}$) and that, mechanistically, charge transport in PVFc/CNT hybrids occurs predominantly via electron hopping between adjacent Fc sites. Moreover, we show that enhancement in β_{Fc} translates into improved performance in several PVFc-based electrochemical applications, including Faradaic energy storage, electrochemically responsive heterogeneous catalysis (ERHC),²¹ and redox moiety-mediated enzymatic sensing.

RESULTS AND DISCUSSION

Enhanced Redox Transformation Efficiency.

PVFc/CNT hybrids with various $r_{\text{C/P}}$ were prepared by a facile solution process²² (Supporting Information (SI) S1.3) that exploits the π -stacking interaction between Fc and CNTs.²³ Figure 2a shows β_{Fc} determined using chronoamperometry (SI S2), as a function of $r_{\text{C/P}}$. β_{Fc} increased monotonically with $r_{\text{C/P}}$ between 0 and 0.4, suggesting a series of intermediate levels of accessibility of the Fc moieties. β_{Fc} appeared to reach a maximum value of ~ 0.67 with $r_{\text{C/P}} = 0.4$. The observed increase in β_{Fc} may be attributed to (i) significantly enhanced electrical conductivities upon addition of CNTs (10^7 -fold increase with $r_{\text{C/P}}$ going from 0 to 0.2, Figure 2b) and (ii) an increasingly porous nanostructure, as evidenced by the increase in the specific surface area (SSA) determined by nitrogen adsorption/desorption isotherm measurements (Figure 2c) and high-resolution scanning electron microscopy (HRSEM) (Figure 2d); such a porous structure could facilitate ion diffusion and increase the polymer/solution interfacial area.

Charge Transport Mechanism. A key issue in the development of EAP systems is the elucidation of the charge propagation mechanism. For Fc-containing polymeric systems that display a diffusive charge transport behavior, a quantitative relationship between the peak current (i_p) during cyclic voltammetric (CV) scans and β_{Fc} has been suggested by Akhoury et al.²⁴ based on the Blauch-Saveant (BS) mean-field model (see SI S4 for details)²⁵

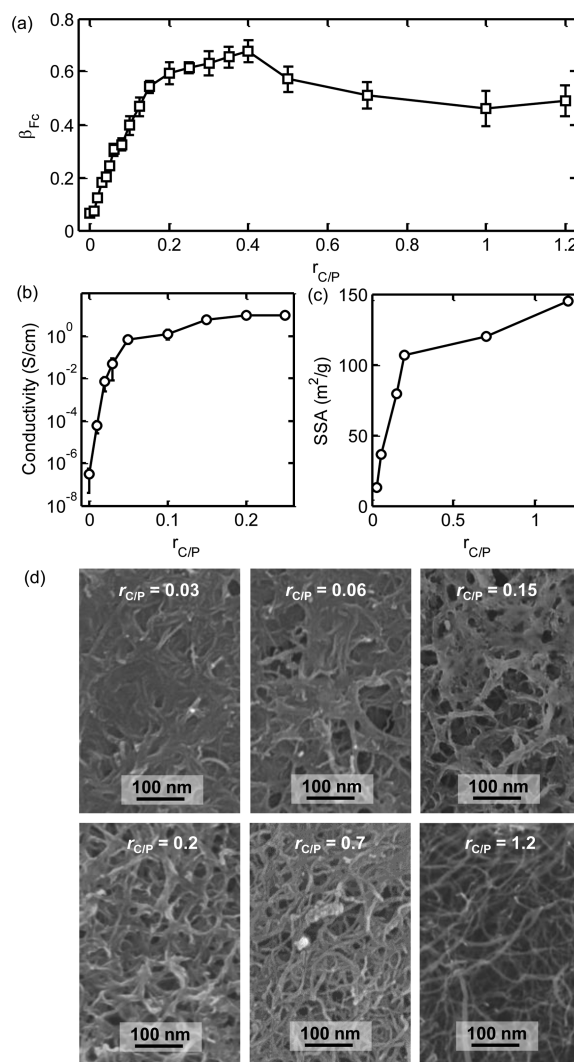


Figure 2. (a) β_{Fc} values as a function of $r_{\text{C/P}}$. (b) Electrical conductivities of the PVFc/CNT films as a function of $r_{\text{C/P}}$. (c) SSA as a function of $r_{\text{C/P}}$. (d) HRSEM images of PVFc/CNT hybrids with various $r_{\text{C/P}}$ values.

$$i_p = \kappa \left(3 \frac{\omega^2}{\beta_{\text{Fc}}^{2n}} + \delta^2 \right) \beta_{\text{Fc}}^{1.5} \nu_s^{0.5} \quad (1)$$

where κ , ω , and n are fitting parameters, ν_s is the CV scan rate, and δ is the electron hopping distance between redox moieties ($\delta = 0.6$ nm for Fc^{24,26}). The BS model interrogates the interdependence of charge propagation between adjacent redox sites (i.e., electron hopping) and the restricted physical movement of redox sites due to thermal motion (i.e., bounded diffusion) to bring the redox sites close enough to permit this electron hopping. When the physical motion is slow, the charge propagation occurs mainly via electron hopping. If the density of redox sites is lower than a critical value so that clusters are disconnected, charge transport should be impossible. However, the physical movement of the redox-active sites around their equilibrium positions, if sufficiently fast, may permit transient rearrangement of the clusters to bring redox sites within the electron hopping distance of each other, enabling charge propagation through bounded diffusion. The first and second terms in the bracket in eq 1 correspond to the bounded diffusion and electron hopping contributions, respectively.

To study the charge transport behavior of PVFc/CNT, we performed CV measurements at different ν_s . Figure 3a shows

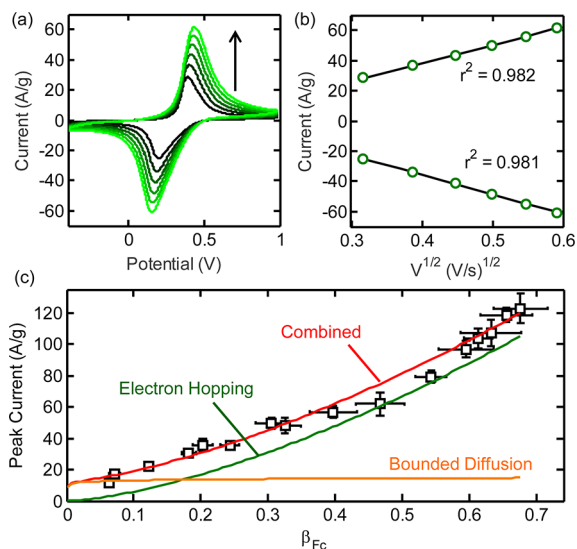


Figure 3. (a) CNT-background subtracted CV curves for a PVFc/CNT hybrid ($r_{C/P} = 0.05$). With the arrow direction, the scan rate is 0.15, 0.2, 0.25, 0.3, and 0.35 V/s. (b) Anodic and cathodic peak currents (open circles) from CV measurements versus the square root of the scan rate. The solid lines are the linear fits. (c) Experimental $i_p - \beta_{Fc}$ data (black squares) at $\nu_s = 0.25$ V/s with the best-fit mean field model described by eq 1 (red line). The green and orange lines show the individual electron hopping and bounded diffusion contributions, respectively.

the CV profiles at various scan rates for a PVFc/CNT hybrid with $r_{C/P} = 0.05$. When ν_s increased, the anodic and cathodic peak potentials shifted to more positive and negative positions, respectively, indicating a resistance-induced potential drop. The linearity between i_p and $\nu_s^{1/2}$ (Figure 3b) suggests diffusion-controlled charge transport. CV profiles and the corresponding

linear relationship between i_p and $\nu_s^{1/2}$ for several other PVFc/CNT hybrids with various $r_{C/P}$ values also support this conclusion (SI S3). Therefore, eq 1 can be used to investigate the charge propagation mechanism within PVFc/CNT systems. We fitted all $i_p - \beta_{Fc}$ data at different ν_s using only one set of parameters (κ , ω , n). Figure 3c depicts the individual contributions from electron hopping and bounded diffusion for a representative set of $i_p - \beta_{Fc}$ data obtained at $\nu_s = 0.25$ V/s. From Figure 3c we conclude that electron hopping is the dominant charge transport mode in the PVFc/CNT hybrids. The detailed fitting procedure and data obtained at other ν_s are presented in SI S4.

To highlight the importance of enhancing the RTE in RPs, we show that the improvement in β_{Fc} translated to enhanced performance of PVFc-based energy storage, ERHC, and enzymatic sensing.

Faradaic Energy Storage. Incorporation of conductive components (e.g., CNTs) into EAPs (in most cases, ICPs) has been widely reported to lead to enhanced energy storage performance of the resulting hybrid materials.²⁷ Because RPs exhibited fundamentally different redox behaviors from ICPs, here we devoted our attention to the question as to whether the RTE of RPs can explain the variation of energy storage capabilities upon incorporation of CNTs. Since the CV profile of PVFc (e.g., Figure 3a) showed pronounced redox peaks, specific capacity (C/g), instead of specific capacitance (F/g), should be used to describe the charge storage properties of PVFc.^{28,29} For ICPs, the theoretical gravimetric specific capacity (C_M , C/g) is $C_M = \alpha F/M_{\text{mon}}$ ^{14,15} where F is the Faraday constant and M_{mon} is the molecular weight of the monomeric unit. In contrast to ICPs, RPs have unambiguous α values ($\alpha = 1$ for PVFc). More importantly, for PVFc, it is β_{Fc} , not α , that dictates the energy storage capabilities. Thus, the theoretical capacity of PVFc should be expressed as $C_M = \beta_{Fc} F/M_{\text{mon}}$. For the PVFc/CNT hybrids, allowing also for the capacitance contribution from CNTs, the total specific capacity can be calculated as

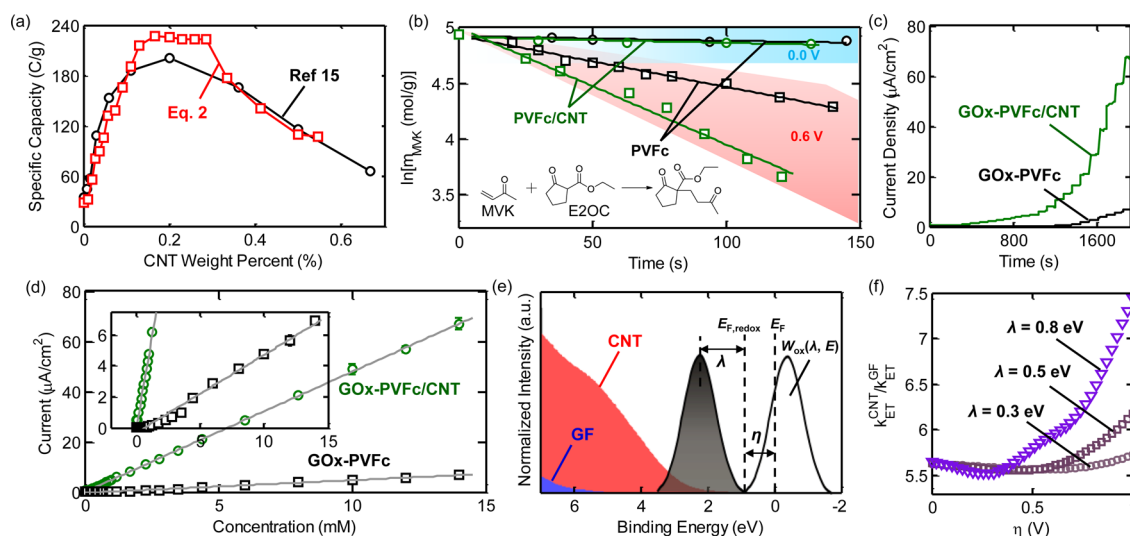


Figure 4. (a) Theoretical capacities of PVFc/CNT hybrids calculated from eq 2, together with the reported values from ref 15. (b) $\ln m_{\text{MVK}}$ versus reaction time for PVFc and PVFc/CNT when the potential was programmed to be 0.0 or 0.6 V. Inset shows the reaction scheme between MVK and E2OC. (c) Amperometric responses of GOx-PVFc and GOx-PVFc/CNT at 0.4 V to successive additions of glucose and (d) corresponding calibration curves (inset shows the low concentration range). (e) UPS spectra for CNTs and GFs near E_F , together with $W_{\text{ox}}(\lambda, E)$ for Fc. (f) $k_{\text{ET}}^{\text{CNT}}/k_{\text{ET}}^{\text{GF}}$ versus η for three different λ values (0.3, 0.5, and 0.8 eV).

$$C_M = \frac{1}{1 + r_{C/P}} \frac{\beta_{Fc} F}{M_{\text{mon}}} + \frac{r_{C/P}}{1 + r_{C/P}} C_{\text{CNT}} \Delta V \quad (2)$$

where C_{CNT} is the specific capacitance of CNTs (16 F/g for the sample used here), and ΔV is the potential range. For PVFc, $M_{\text{mon}} = 212.07$ g/mol and $\Delta V = 0.6$ V. Figure 4a depicts the theoretical capacities (red squares) calculated from eq 2, together with the previously measured values (black circles).²² These two sets of data are in general agreement, indicating that the $r_{C/P} - \beta_{Fc}$ relationship explains the composition-dependent energy storage performance of PVFc/CNT hybrids.

Electrochemically Responsive Heterogeneous Catalysis. ERHC is a method to control reaction kinetics by using electrochemical potential to manipulate the concentration of catalytically active sites. For PVFc-based ERHC systems, the number of active Fc molecules should play an important role in the catalytic performance. The model reaction we chose for comparing the ERHC performance of PVFc/CNT and PVFc systems is the Michael reaction of ethyl-2-oxocyclopentane carboxylate (E2OC) and methyl vinyl ketone (MVK) (Figure 4b inset), which is pseudo-first-order in MVK.³⁰ The oxidized form of Fc (i.e., ferrocenium) acts as a Lewis acid to catalyze this reaction, whereas Fc, in the reduced form, exhibits no such activity.³⁰ As is the convention in heterogeneous catalysis, the reaction rate is expressed as moles of reactants consumed per unit catalyst mass.³¹ Here the rate law is expressed as $-r$ (mol/(g catalyst·min)) = $-dm_{\text{MVK}}/dt = k_{\text{app}} m_{\text{MVK}}$, where m_{MVK} (mol/g) is the MVK concentration normalized to the PVFc mass, and k_{app} is the apparent rate constant (min⁻¹). Figure 4b shows $\ln m_{\text{MVK}}$ versus the reaction time using PVFc/CNT ($r_{C/P} = 0.3$) or PVFc alone as the ERHC-type catalyst; the polymer mass was the same in both systems. When we applied a potential of 0.0 V (reduced state), m_{MVK} did not change over time. By contrast, when the potential was increased to 0.6 V (oxidized state), m_{MVK} decreased significantly. The difference in reaction kinetics when applying different potentials indicates the electrochemically controlled catalytic activities for both PVFc and PVFc/CNT. More importantly, at 0.6 V, m_{MVK} decayed faster with PVFc/CNT than with PVFc. The faster decay is indicative of the accelerated kinetics using PVFc/CNT, which contains more accessible Fc sites. For PVFc, with four independent measurements we determined that $k_{\text{app}}^{0.6\text{ V}} = (4.1 \pm 0.7) \times 10^{-3}$ min⁻¹, whereas for PVFc/CNT, we obtained a larger value for $k_{\text{app}}^{0.6\text{ V}}$ of $(11.5 \pm 1.2) \times 10^{-3}$ min⁻¹.

Redox Moiety-Mediated Enzymatic Sensing. For enzymatic biosensing, electron transfer between an enzyme and an electrode surface is often hindered by the insulating protein shell around the metal center of the enzyme, such as is the case in glucose oxidase (GOx)-based sensing.³² Fc can function as a redox mediator to facilitate the electron transfer process between GOx and electrodes (for details, see SI S1.5). To explore the effects of RTE of PVFc on sensing, we prepared two different types of glucose sensors by immobilizing GOx onto PVFc or PVFc/CNT ($r_{C/P} = 0.2$) electrodes, denoted as GOx-PVFc and GOx-PVFc/CNT, respectively. Figure 4c shows that, compared to GOx-PVFc, GOx-PVFc/CNT exhibited significantly higher current responses to successive additions of glucose from 0.1 to 14 mM. The calibration curves (Figure 4d) show that the sensitivity was significantly higher when using GOx-PVFc/CNT ($4.79 \mu\text{A}/\text{cm}^2/\text{mM}$) than GOx-PVFc ($0.51 \mu\text{A}/\text{cm}^2/\text{mM}$). The detection limits of GOx-PVFc/CNT and GOx-PVFc, determined at a signal-to-noise ratio of 3 (SI S1.5), were 0.013 and 0.17 mM, respectively. One

explanation for this improved sensing performance in GOx-PVFc/CNT is that a higher β_{Fc} permits a more efficient mediation process because more active Fc moieties are accessible for communicating electrons with GOx.

Another important factor may be the enhanced electron transfer kinetics between Fc and the electrode; it has been found that a faster electron transfer process with Fc redox mediators in GOx-based sensors leads to improved sensing performance.³³ Also, an understanding of the effects of incorporating nanotubes into PVFc on heterogeneous electron transfer kinetics may be of importance for other applications involving Fc electrochemistry, such as dye sensitized solar cells³⁴ and Faradaic energy storage devices.²² We suspect that accelerated electron transfer may occur in GOx-PVFc/CNT due to the incorporation of CNTs that are rich in π -electrons and have a high density of electronic states (DOS) near the Fermi level (E_F). In GOx-PVFc, without CNTs, slower electron transfer occurs between Fc and the graphite fiber (GF) substrate, which presumably exhibits a lower DOS near E_F (ρ_F). To elucidate the electron transfer kinetics quantitatively, we performed calculations using the Gerisher-Marcus (GM) theory, according to which

$$k_{\text{ET}} = \xi \int_{-\infty}^{\infty} \theta(E) f(E) \rho_F(E) W_{\text{ox}}(\lambda, E) dE \quad (3)$$

$$W_{\text{ox}}(\lambda, E) = \frac{1}{\sqrt{4\pi k_B T \lambda}} \exp\left(-\frac{(E - E_{F,\text{redox}} - \lambda)^2}{4\pi k_B T \lambda}\right) \quad (4)$$

where k_{ET} is the electron transfer rate constant, ξ is the prefactor, $\theta(E)$ is the proportionality function, $\rho_F(E)$ is the DOS near E_F , $f(E)$ is the Fermi-Dirac distribution, $W_{\text{ox}}(\lambda, E)$ is the energy distribution function of the unoccupied states of Fc/Fc⁺, k_B is the Boltzmann constant, $E_{F,\text{redox}}$ is the Fermi level of Fc/Fc⁺, and λ is the solvent reorganization energy for Fc, which ranges from 0.3 to 1 eV.³⁵ Usually it is assumed that $\theta(E)$ is independent of energy, and ξ is not specific to CNTs or GFs,^{36,37} and hence that they cancel out when we calculate the relative rate constants. ρ_F for CNTs and GFs was approximated by the intensities of the valence bands near E_F , measured by ultraviolet photoelectron spectroscopy (UPS). Figure 4e depicts the detailed UPS spectra near E_F of CNTs and GFs, together with W_{ox} for Fc. The overall UPS spectra and the energy diagrams of CNTs, GFs, and Fc are presented in SI S5. It is evident that CNTs exhibit a significantly higher ρ_F than do GFs. The ratios of the calculated rate constants obtained with CNTs and GFs ($k_{\text{ET}}^{\text{CNT}}/k_{\text{ET}}^{\text{GF}}$) as a function of overpotential (η) at three different λ values (0.3, 0.5, and 0.8 eV) are shown in Figure 4f. These results indicate that, relative to the k_{ET} values for GFs, those for CNTs are ~ 5.5 – 7.5 -fold larger for η ranging from 0 to 1 eV.

CONCLUSIONS

This study investigates, for the first time, the RTE of unconjugated EAPs with discrete electron donor/acceptors. We report an effective method to improve the RTE of RPs by incorporating conductive nanomaterials and highlight the significance of enhancing RTE in several important electrochemical processes. With controllable electrochemical activities and ease of fabrication via a facile, scalable solution process, the PVFc/CNT hybrids may find a variety of applications, while the redox transformation efficiency of ferrocene governs device performance.

Our study also provides useful insights into the charge transport mechanism of RP/carbon hybrids and the accelerated ET kinetics by incorporation of materials with a high DOS near E_F . Other types of carbon materials with tunable electronic structure^{38,39} could also be combined with RPs to manipulate their RTE, suggestive of potential design flexibility.

Furthermore, this report suggests an important and generalizable strategy to modulate the accessibility and utilization of redox moieties in RP systems through creation of a heterogeneous nanostructure with a RP-coated porous conducting framework that will simultaneously facilitate electron and ion transport processes. The conductive scaffold provides efficient electron-conducting pathways. The nanoporous architecture serves to (i) reduce significantly ion diffusion length scales and (ii) increase the RP/solution interfacial area to make more redox moieties accessible for electrochemical transformation. Hence we expect that other nanostructured RP/conductor hybrids, such as electrochemically constructed RP/ICP nanocomposites,⁴⁰ may also display enhanced RTE and thus, potentially, could be used for a myriad of applications, such as energy storage, ERHC, and biosensing.

■ ASSOCIATED CONTENT

● Supporting Information

The Supporting Information is available free of charge on the ACS Publications website at DOI: 10.1021/acs.chemmater.5b03957.

Experimental details, determination of β_{FC} diffusion controlled charge transport of PVFc/CNT hybrids, the $i_p - \beta_{FC}$ data fitting procedure, and overall UPS spectra and energy diagrams (PDF)

■ AUTHOR INFORMATION

Corresponding Author

*E-mail: tahatton@mit.edu.

Notes

The authors declare no competing financial interest.

■ ACKNOWLEDGMENTS

This research was partially supported by a grant from the MIT Energy Initiative Seed Fund program. X.M. was supported by a Skoltech Fellowship.

■ REFERENCES

- (1) Pron, A.; Gawrys, P.; Zagorska, M.; Djurado, D.; Demadrille, R. Electroactive materials for organic electronics: preparation strategies, structural aspects and characterization techniques. *Chem. Soc. Rev.* **2010**, *39*, 2577–2632.
- (2) Ramuz, M.; Hama, A.; Huerta, M.; Rivnay, J.; Leleux, P.; Owens, R. M. Combined Optical and Electronic Sensing of Epithelial Cells Using Planar Organic Transistors. *Adv. Mater.* **2014**, *26*, 7083–7090.
- (3) Nagaraju, D. H.; Rebis, T.; Gabrielsson, R.; Elfving, A.; Milczarek, G.; Ingnas, O. Charge Storage Capacity of Renewable Biopolymer/Conjugated Polymer Interpenetrating Networks Enhanced by Electroactive Dopants. *Adv. Energy Mater.* **2014**, *4*, 4.
- (4) Svirskis, D.; Trivas-Sejdic, J.; Rodgers, A.; Garg, S. Electrochemically controlled drug delivery based on intrinsically conducting polymers. *J. Controlled Release* **2010**, *146*, 6–15.
- (5) Fattahi, P.; Yang, G.; Kim, G.; Abidian, M. R. A Review of Organic and Inorganic Biomaterials for Neural Interfaces. *Adv. Mater.* **2014**, *26*, 1846–1885.

- (6) Savéant, J. M. Electron hopping between fixed sites: Equivalent diffusion and migration laws. *J. Electroanal. Chem. Interfacial Electrochem.* **1986**, *201*, 211–213.

- (7) Laviron, E. A multilayer model for the study of space distributed redox modified electrodes: Part I. Description and discussion of the model. *J. Electroanal. Chem. Interfacial Electrochem.* **1980**, *112*, 1–9.

- (8) Vorotyntsev, M. A.; Vasilyeva, S. V. Metallocene-containing conjugated polymers. *Adv. Colloid Interface Sci.* **2008**, *139*, 97–149.

- (9) Dalton, E. F.; Surridge, N. A.; Jernigan, J. C.; Wilbourn, K. O.; Facci, J. S.; Murray, R. W. Charge transport in electroactive polymers consisting of fixed molecular redox sites. *Chem. Phys.* **1990**, *141*, 143–157.

- (10) Inzelt, G. *Conducting polymers: a new era in electrochemistry*, 2nd ed.; Springer: Heidelberg, New York, 2012; p ix, 309 p.

- (11) Gabrielli, C.; Perrot, H. AC-Electrogravimetry Investigation in Electroactive Thin Films. *Mod. Aspects Electrochem.* **2009**, *44*, 151–238.

- (12) *Advances in Chemical Physics: Polymeric Systems*; John Wiley & Sons, Inc.: 1996; Vol. 94.

- (13) Blauch, D. N.; Saveant, J. M. Dynamics of Electron Hopping in Assemblies of Redox Centers - Percolation and Diffusion. *J. Am. Chem. Soc.* **1992**, *114*, 3323–3332.

- (14) Peng, C.; Zhou, X.; Chen, G. Z.; Moggia, F.; Fages, F.; Brisset, H.; Roncali, J. Internally referenced analysis of charge-transfer reactions in a new ferrocenyl bithiophenic conducting polymer through cyclic voltammetry. *Chem. Commun.* **2008**, 6606–6608.

- (15) Peng, C.; Hu, D.; Chen, G. Z. Theoretical specific capacitance based on charge storage mechanisms of conducting polymers: Comment on 'Vertically oriented arrays of polyaniline nanorods and their super electrochemical properties'. *Chem. Commun.* **2011**, *47*, 4105–4107.

- (16) Zotti, G.; Zecchin, S.; Schiavon, G.; Berlin, A.; Pagani, G.; Canavesi, A. Conductivity in redox modified conducting polymers 0.2. Enhanced redox conductivity in ferrocene-substituted polypyrroles and polythiophenes. *Chem. Mater.* **1995**, *7*, 2309–2315.

- (17) *Applications of Electroactive Polymers*; Chapman & Hall: 1993; p 354.

- (18) Zhang, Y. X.; Kim, J. J.; Chen, D.; Tuller, H. L.; Rutledge, G. C. Electrospun Polyaniline Fibers as Highly Sensitive Room Temperature Chemiresistive Sensors for Ammonia and Nitrogen Dioxide Gases. *Adv. Funct. Mater.* **2014**, *24*, 4005–4014.

- (19) Scrosati, B. *Applications of electroactive polymers*, 1st ed.; Chapman & Hall: London, New York, 1993; p xiii, 354 p.

- (20) Chen, T.; Wang, L.; Jiang, G. H.; Wang, J. J.; Dong, X. C.; Wang, X. J.; Zhou, J. F.; Wang, C. L.; Wang, W. Electrochemical behavior of poly(ferrocenyldimethylsilane-beta-dimethylsiloxane) films. *J. Phys. Chem. B* **2005**, *109*, 4624–4630.

- (21) Mao, X.; Tian, W.; Wu, J.; Rutledge, G. C.; Hatton, T. A. Electrochemically Responsive Heterogeneous Catalysis for Controlling Reaction Kinetics. *J. Am. Chem. Soc.* **2015**, *137*, 1348–1355.

- (22) Mao, X.; Simeon, F.; Achilleos, D. S.; Rutledge, G. C.; Hatton, T. A. Metallocene/carbon hybrids prepared by a solution process for supercapacitor applications. *J. Mater. Chem. A* **2013**, *1*, 13120–13127.

- (23) Mao, X.; Rutledge, G. C.; Hatton, T. A. Polyvinylferrocene for Noncovalent Dispersion and Redox-Controlled Precipitation of Carbon Nanotubes in Nonaqueous Media. *Langmuir* **2013**, *29*, 9626–9634.

- (24) Akhoury, A.; Bromberg, L.; Hatton, T. A. Interplay of Electron Hopping and Bounded Diffusion during Charge Transport in Redox Polymer Electrodes. *J. Phys. Chem. B* **2013**, *117*, 333–342.

- (25) Blauch, D. N.; Saveant, J. M. Dynamics of electron hopping in assemblies of redox centers. Percolation and diffusion. *J. Am. Chem. Soc.* **1992**, *114*, 3323–3332.

- (26) Bu, H.-Z.; English, A. M.; Mikkelsen, S. R. Charge Transport in Ferrocene-Containing Polyacrylamide-Based Redox Gels. *J. Phys. Chem. B* **1997**, *101*, 9593–9599.

- (27) Liu, R.; Duay, J.; Lee, S. B. Heterogeneous nanostructured electrode materials for electrochemical energy storage. *Chem. Commun.* **2011**, *47*, 1384–1404.

- (28) Brousse, T.; Belanger, D.; Long, J. W. To Be or Not To Be Pseudocapacitive? *J. Electrochem. Soc.* **2015**, *162*, A5185–A5189.
- (29) Akinwolemiwa, B.; Peng, C.; Chen, G. Z. Redox Electrolytes in Supercapacitors. *J. Electrochem. Soc.* **2015**, *162*, A5054–A5059.
- (30) Durkee, D. A.; Eitouni, H. B.; Gomez, E. D.; Ellsworth, M. W.; Bell, A. T.; Balsara, N. R. Catalysts from self-assembled organometallic block copolymers. *Adv. Mater.* **2005**, *17*, 2003.
- (31) Fogler, H. S. *Elements of chemical reaction engineering*, 4th ed.; Prentice Hall PTR: Upper Saddle River, NJ, 2006; p xxxii, 1080 p.
- (32) Dey, R. S.; Raj, C. R. Redox-Functionalized Graphene Oxide Architecture for the Development of Amperometric Biosensing Platform. *ACS Appl. Mater. Interfaces* **2013**, *5*, 4791–4798.
- (33) Liu, J. Y.; Wang, X. H.; Wang, T. S.; Li, D.; Xi, F. N.; Wang, J.; Wang, E. K. Functionalization of Monolithic and Porous Three-Dimensional Graphene by One-Step Chitosan Electrodeposition for Enzymatic Biosensor. *ACS Appl. Mater. Interfaces* **2014**, *6*, 19997–20002.
- (34) Daeneke, T.; Kwon, T.-H.; Holmes, A. B.; Duffy, N. W.; Bach, U.; Spiccia, L. High-efficiency dye-sensitized solar cells with ferrocene-based electrolytes. *Nat. Chem.* **2011**, *3*, 211–215.
- (35) Orłowski, G. A.; Chowdhury, S.; Kraatz, H. B. Reorganization energies of ferrocene-peptide monolayers. *Langmuir* **2007**, *23*, 12765–12770.
- (36) Heller, I.; Kong, J.; Williams, K. A.; Dekker, C.; Lemay, S. G. Electrochemistry at single-walled carbon nanotubes: The role of band structure and quantum capacitance. *J. Am. Chem. Soc.* **2006**, *128*, 7353–7359.
- (37) Sharma, R.; Baik, J. H.; Perera, C. J.; Strano, M. S. Anomalously Large Reactivity of Single Graphene Layers and Edges toward Electron Transfer Chemistries. *Nano Lett.* **2010**, *10*, 398–405.
- (38) Mao, X.; Simeon, F.; Rutledge, G. C.; Hatton, T. A. Electrospun Carbon Nanofiber Webs with Controlled Density of States for Sensor Applications. *Adv. Mater.* **2013**, *25*, 1309–1314.
- (39) Mao, X.; Rutledge, G. C.; Hatton, T. A. Nanocarbon-based electrochemical systems for sensing, electrocatalysis, and energy storage. *Nano Today* **2014**, *9*, 405–432.
- (40) Tian, W.; Mao, X.; Brown, P.; Rutledge, G. C.; Hatton, T. A. Electrochemically Nanostructured Polyvinylferrocene/Polypyrrole Hybrids with Synergy for Energy Storage. *Adv. Funct. Mater.* **2015**, *25*, 4803–4813.